

Granular superconductivity at room temperature in bulk highly oriented pyrolytic graphite samples

T. Scheike, P. Esquinazi¹, A. Setzer and W. Böhlmann

^a*Division of Superconductivity and Magnetism, Institut für Experimentelle Physik II, Universität Leipzig, Linnéstraße 5, D-04103 Leipzig, Germany*

Abstract

We have studied the magnetic response of two bulk highly oriented pyrolytic graphite (HOPG) samples with different internal microstructure. For the sample with well defined interfaces, parallel to the graphene layers, the temperature and magnetic field hysteresis are similar to those found recently in water-treated graphite powders. The observed behavior indicates the existence of granular superconductivity above room temperature in agreement with previous reports in other graphite samples. The granular superconductivity behavior is observed only for fields normal to the embedded interfaces, whereas no relevant hysteresis in temperature or field is observed for fields applied parallel to them. Increasing the temperature above ~ 400 K changes irreversibly the hysteretic response of the sample.

1. Introduction

Since the observation of superconductivity in potassium intercalated graphite $C_8K[1]$, a considerable amount of studies reported this phenomenon in graphite

¹Corresponding author. Tel/Fax: +49 341 9732751/69. E-mail address: esquin@physik.uni-leipzig.de (P. Esquinazi)

based compounds with critical temperatures $T_c \sim 10$ K, in intercalated graphite[2, 3], and above 30 K - though not percolative - in certain HOPG samples[4, 5] as well as in doped graphite [6–10]. Theoretical work that deals with superconductivity in graphite and in graphene has been published in recent years, e.g., *p*-type superconductivity predicted in inhomogeneous regions of the graphite structure [11] or *d*-wave high- T_c superconductivity[12] based also on resonance valence bonds[13], or at the graphite surface region due to a topologically protected flat band[14, 15]. Following a BCS approach in two dimensions (with anisotropy) critical temperatures $T_c \sim 60$ K have been estimated if the density of conduction electrons per graphene plane increases to $n \sim 10^{14}$ cm⁻², a density that might be induced by defects and/or hydrogen ad-atoms[16] or by Li deposition[17]. Further predictions for superconductivity in graphene support the premise that $n > 10^{13}$ cm⁻² in order to reach $T_c > 1$ K[18, 19].

While the existence of defect-induced magnetic order in graphite reported in [4, 20] was later confirmed by independently done studies [21–31], the reproducibility of the phenomenon of high temperature superconductivity found in some bulk ordered graphite samples reported previously [4] remain a real challenge. It has been recently shown that water-treated graphite powder (WTGP) provides clear signs for granular superconductivity at temperatures above 300 K [32]. In spite of a small superconducting yield, too small to get any information about the corresponding superconducting phase(s), the observed behavior resembled the one expected for a system of Josephson coupled superconducting grains with critical temperature above room temperature [32]. These last results support earlier reports on the existence of

room-temperature superconductivity in disordered graphite powders [33, 34] and in HOPG samples [4, 10].

Recently performed transport measurements on different graphite samples of different thickness [35–38] as well as in transmission electron microscope (TEM) lamellae of HOPG samples [39, 40] suggest that the superconducting regions should be located at some interfaces between crystalline graphite regions, running parallel to the graphene planes. We note that superconductivity has been found at the interfaces between oxide insulators [41] as well as between metallic and insulating copper oxides with $T_c \gtrsim 50$ K[42]. In case of doped semiconductors the interfaces in Bi-bicrystals of inclination type show superconductivity up to 21 K, although Bi bulk is not a superconductor[43].

The aim of this experimental work is then the study of the magnetic irreversibility (in temperature T as well as in magnetic field H) of HOPG bulk samples and compare it with the one reported for WTGP. We show that for magnetic fields applied normal to the internal interfaces of a HOPG sample the obtained behavior is similar to that found in WTGP but with some interesting differences. Increasing the temperature of the sample above 400 K changes the hysteretic response in an irreversible way. For a second HOPG sample without those interfaces we did not find any relevant irreversibility in T or H . Our results support the view that the superconducting regions are quasi-two dimensional and localized very likely at the embedded interfaces, recently found to exist in some HOPG samples [35, 36], running parallel to the graphene planes of the graphite structure.

2. Experimental details and samples characteristics

Magnetic moment measurements of two HOPG samples from different batches, both nominally ZYA grade (Advanced Ceramics, now Momentive Performance Materials Inc.), were performed using a commercial MPMS-7 SQUID magnetometer. The magnetic impurity concentration determined by PIXE for these samples is below 1 ppm, see for example [26, 44], with excellent reproducibility for all samples of the same grade. Before the magnetic measurements were done, the samples surface layers were removed with scotch tape and afterwards they were cleaned in an ultrasonic bath. The masses of the samples and size (length \times width \times thickness) were: $m \simeq 1.3$ mg ($\sim 3 \times 2 \times 1$ mm³) for the HOPG-1 and $\simeq 2.3$ mg ($\sim 4 \times 3 \times 0.8$ mm³) for the HOPG-2 sample. Each sample was fixed on the middle of a long quartz glass stick, especially designed to reduce to a minimum any magnetic contribution from the sample holder. The magnetic moment measurements were performed with the applied magnetic field parallel to the c -axis of the HOPG samples. A few measurements were performed also with the field parallel to the graphene planes to check for the anisotropic response of the signals, as was found in [4]. Hysteresis were measured at different temperatures in zero-field-cooled (ZFC) and field-cooled (FC) states at different applied fields as well as a function of field at constant temperatures. For temperatures above 390 K an available SQUID oven was used.

Although both HOPG samples show an apparent similar Bernal ordered structure as well as similar diamagnetic background signals, we show below that the observed irreversibilities in field and temperature are related to the internal structure of the samples, in particular to the existence of the internal

interfaces, as proposed recently in [35–38, 45]. The results obtained for the studied samples rule out the influence of unknown artifacts of the SQUID as well as of the used background subtraction procedure.

In general the main structural phase of commercial HOPG samples is the Bernal hexagonal one with the AB... stacking sequence along the c -axis. Taking into account theoretical predictions of the existence of high temperature surface superconductivity in rhombohedral graphite [15], it is of interest to check whether the investigated samples, specially the HOPG-1 one, shows some evidence for isolated rhombohedral crystallites. X-rays measurements were done in the two selected HOPG samples with a Philips X’Pert diffractometer. In the wide-angle diffractogram, see Fig. 1(a), only the (002) and (004) reflections are visible. From the Bragg (002) maximum at $2\theta = 26.60^\circ$ we estimate a lattice constant $c = 6.70 \text{ \AA}$. Because the Bragg angle for the [001] family of reflexes for the hexagonal (Bernal) and for the rhombohedral graphite structures is the same, the observed Bragg reflexes do not provide any information about the possible existence of rhombohedral crystallites. According to [46] diffraction peaks at 43.45° and 46.32° were found in graphite bulk samples, which can be ascribed to (10-11) and (10-12) reflections of rhombohedral phase in coexistence within the hexagonal crystalline phase matrix. For our samples and within experimental resolution no diffraction peaks at those angles are observed indicating that the amount of rhombohedral phase should be much smaller than 1%.

A clear difference in the internal structure of the two HOPG samples can be observed via the rocking curve measurement. Rocking curves are primarily used to study defects such as dislocation density, mosaic spread,

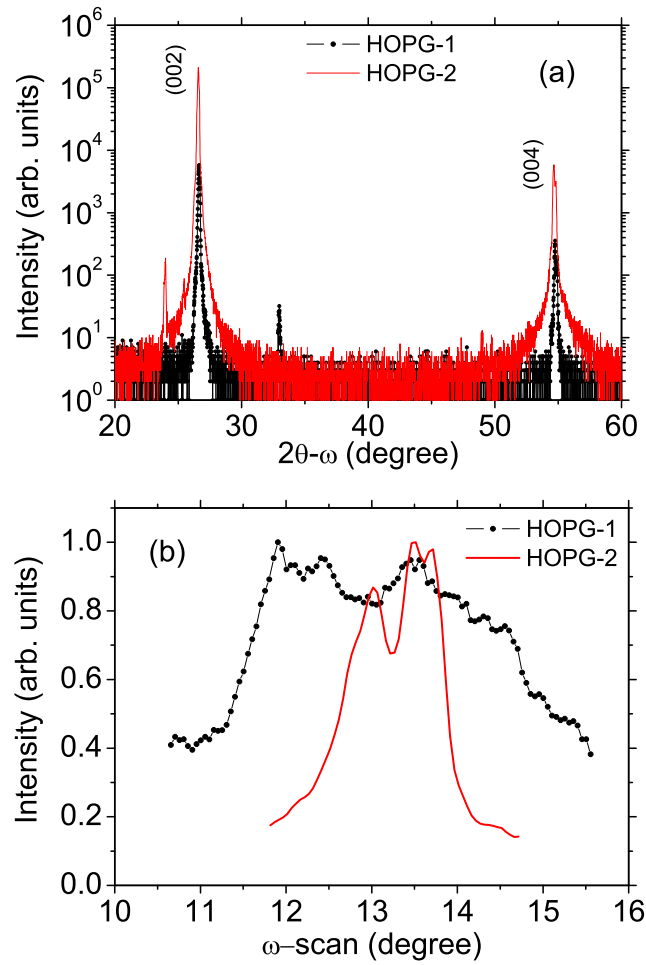


Figure 1: (a) Wide angle diffractogram of the two HOPG samples. (b) Rocking curves of the two HOPG samples at the (002) Bragg peak.

curvature, misorientation and inhomogeneity. A comparison of the rocking curves of samples HOPG-1 and HOPG-2, see Fig. 1(b) clearly indicates that the sample HOPG-1 has a broader rocking curve width. This broadening can come from defects like mosaicity, dislocations, and disruptions in the perfect parallelism of atomic planes, pointing that sample HOPG-1 has a larger “disorder” than the HOPG-2 sample.

Low-energy (20 keV) TEM pictures of the internal microstructure of the two samples are shown in Fig. 2. We have used the same procedure as described in [45, 47, 48] to minimize the influence of Ga^+ ions on the graphite structure during cutting of the lamella. It is interesting to note that already by the cutting of the lamellae using a dual beam microscope (FEI Nanolab XT200) we realized that there was a clear difference between the two samples. Whereas the TEM lamellae of the HOPG-1 sample could be obtained without any special difficulties, this was not the case for the HOPG-2 sample. The HOPG-2 sample got slightly electrically charged during the cutting process. A possible reason for the different behavior could be due to the parallel, high conductivity of the interfaces [36] (or graphene layers with certain lattice defects) that exist in the HOPG-1 sample only. We note that the earlier observed metallic conductivity of graphite is not intrinsic but mainly due to well defined interfaces [35, 36, 45], or lattice defects [49].

A comparison between the TEM pictures obtained for the two samples clearly indicate the existence of interfaces in the HOPG-1 sample. In contrast, the HOPG-2 sample appears much more homogeneous, without clear interface regions, see Fig. 2. The pictures suggest that the difference in the lattice “disorder” observed in X-ray diffraction between the two samples

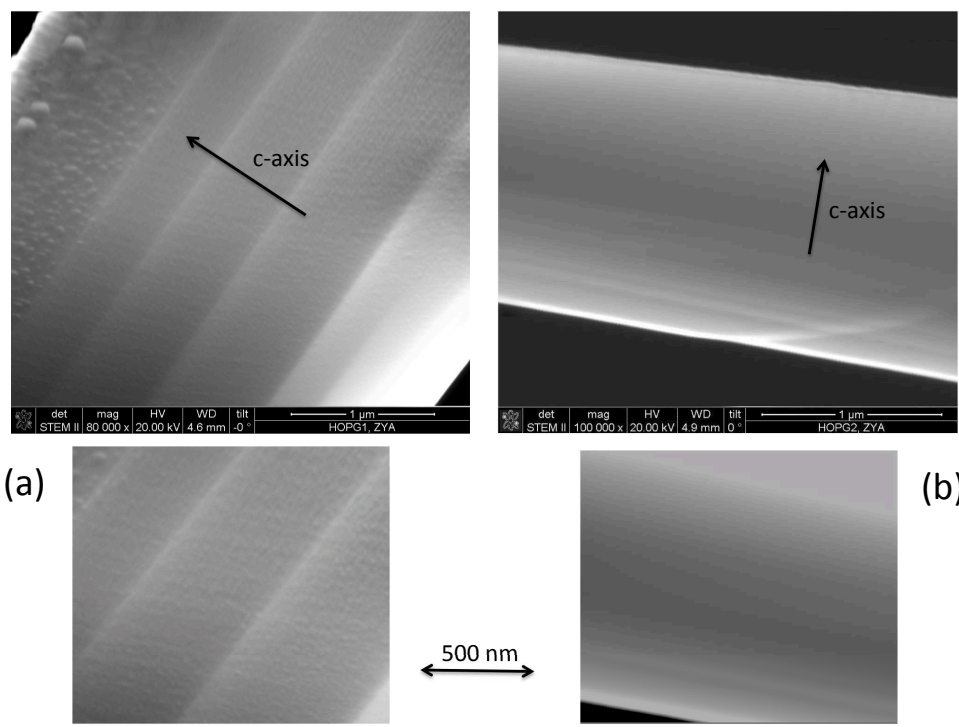


Figure 2: Low energy transmission electron microscope pictures of regions of two lamellae of equal thickness (300 nm) of samples HOPG-1 (a) and HOPG-2 (b) at two different resolutions.

could be related to the existence of a different mosaicity and therefore to the well defined embedded interfaces between crystalline regions of the graphite structure. All these results together with magnetization ones discussed below suggest that the superconducting phase(s) should be at the interfaces or near the interface regions, as recently done transport measurements contacting the edges of these interfaces indicate [45]. The resolution of our TEM does not allow us to get more information on the internal lattice structure within the interface regions. Further studies using HRTEM are necessary to check whether rhombohedral unit cells are embedded at the interfaces, a not simple task indeed. We note however, that the irreversible changes in the hysteretic response, after a temperature annealing of less than one hour below 600 K already suggests that not only the structure behind the interfaces but lattice defects and/or hydrogen may play a role in the observed behavior.

3. Magnetization Results

3.1. Irreversible behavior in temperature at fixed fields

A method that it does not need any background subtraction and allows us to check for an intrinsic irreversibility due to either pinned superconducting fluxons (or vortices) or magnetic domains or magnetocrystalline anisotropy as in the case of ferromagnets, is the measurement of the hysteresis between the magnetic moment $m(T)$ in the FC and ZFC states. The opening between the ZFC- and FC-branches at a field of 7 T applied normal to the graphene layers and interfaces of the HOPG-1 sample can be clearly seen already in the scale of Fig. 3(a). The difference between the FC- and ZFC-branches at different applied fields is shown for this sample in Fig. 3(b).

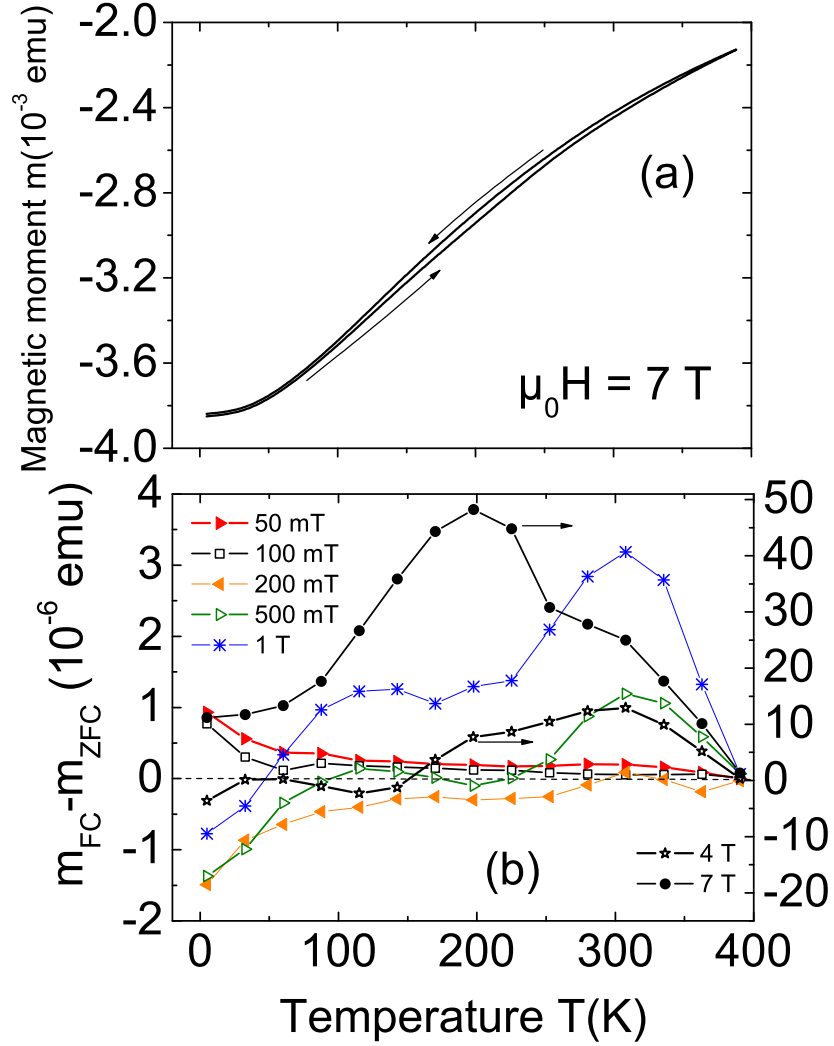


Figure 3: (a) Magnetic moment m vs. temperature at a constant field of $\mu_0 H = 7$ T in ZFC (lower curve) and FC (upper curve) for sample HOPG-1. The field is applied normal to the graphene layers and interfaces of the sample. (b) The difference between FC and ZFC magnetic moment curves at different applied fields for sample HOPG-1. Right y -axis corresponds to the fields of 4 T and 7 T.

For a field of 50 mT the difference between the FC- and ZFC-branches $\Delta m = m_{\text{FC}} - m_{\text{ZFC}}$ is similar to that obtained for the WTGP in [32], in particular the shallow maximum near the turning temperature point (390 K) and the decrease of this difference at 100 mT in the whole temperature range. However, at 200 mT Δm is negative at nearly all temperatures. Such a negative difference has been already seen in WTGP but at temperatures only near the turning temperature point (300 K) and was partially attributed to the influence of flux creep at those high temperatures [32]. However, in the HOPG-1 sample the negative difference even increases at lower temperatures, see Fig. 3(b). This would indicate that the possible superconducting regions shield or expel the applied field stronger (more diamagnetism) when the sample is cooled down in field than when warming in the ZFC state, clearly an unusual behavior in conventional superconductors.

At higher applied fields the magnitude of the maximum $\Delta m(T \simeq 310 \text{ K})$, near the turning temperature point, increases as well as the whole difference in all the temperature range with exception of the low temperature region where the crossing to negative values is observed up to a field of 4 T, see Fig. 3(b). The position of the high-temperature maximum remains field independent, see Fig. 5. A close look at the $\Delta m(T)$ curves at fields $\mu_0 H \geq 200 \text{ mT}$ reveals that maxima at $T \sim 150 \text{ K}$ and at $T \simeq 200 \text{ K}$ develop increasing field.

To assure that the negative values as well as the whole temperature dependence obtained for the difference between FC and ZFC curves are not due to a SQUID artifact, the following measurements were performed at 200 mT using two measurement mode options, namely: (1) a linear regression mode

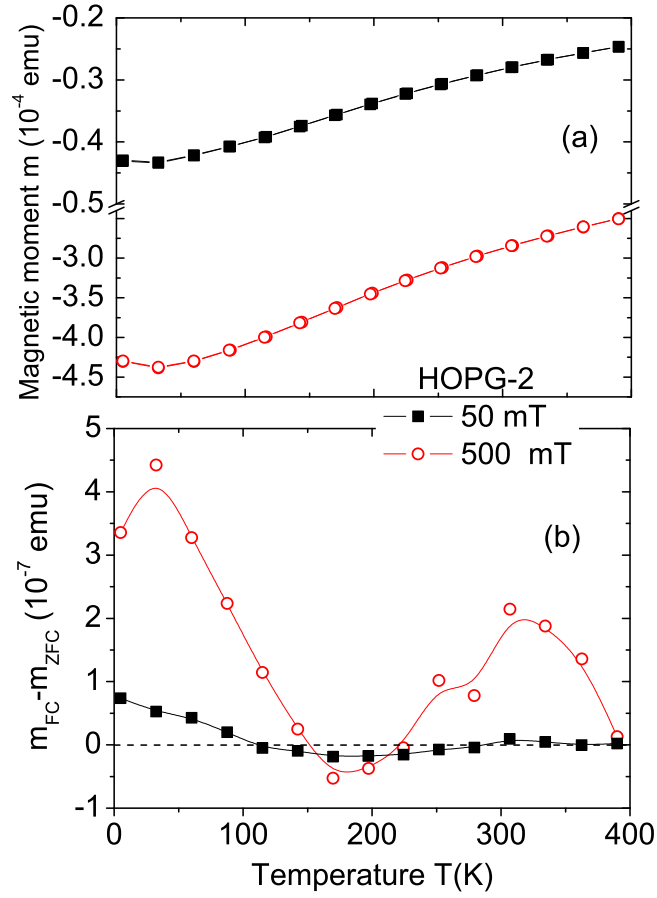


Figure 4: (a) Temperature dependence of the magnetic moment for sample HOPG-2. The curves were obtained in the ZFC (warming) and FC (cooling) states, as for sample HOPG-1, see Fig. 3. (b) The difference $\Delta m(T)$ between the FC and ZFC curves at two applied fields. The difference remains less than $1 \mu\text{emu}$ in the whole temperature range.

and (2) the iterative regression mode. It is known that the linear regression mode can lead to smaller signals compared to the iterative regression mode because only the amplitude of the signal is fitted assuming the sample remains in the center point during the complete measurement [50]. Therefore, data were obtained with the two methods to exclude errors due to a possible shift of the sample during the measurements. The results (not shown) reveal a small difference between the two mode curves, i.e. the linear regression mode curve is smaller than the iterative one with a maximum difference of $0.2\mu\text{emu}$, much smaller than the differences observed, see Fig. 3. This small difference might be due to a displacement of the sample center position determined by the regression mode.

To further rule out that the observed irreversibility in temperature is not related to artifacts but is due to intrinsic sample properties, especially at low fields $\mu_0 H < 1$ T where this irreversibility is of the order of $\sim 1 \mu\text{emu}$ (see Fig. 3(b)), the ZFC and FC curves have been measured also for the HOPG-2 sample, see Fig. 4. The obtained $\Delta m(T)$ remains well below $1 \mu\text{emu}$ at all temperatures, see Fig. 4(b). This result agrees with the absence of a field hysteresis in sample HOPG-2, see Sec. 3.2 below.

An opening of the ZFC-FC curves is usually associated with pinning of magnetic entities starting at a field dependent irreversible temperature. As noted in the measurements of the WTGP in [32], the differences between FC and ZFC shown in Fig. 3 for the HOPG-1 sample and for fields normal to the interfaces do not appear to be compatible to the hysteresis one expects from magnetic order of ferromagnetic large as well as nanoparticles in the sample, see for example [51]. Furthermore, the amount of magnetic impurities in

our samples is too low to account for the measured hysteresis in temperature and field and, more important, the irreversibility is observed only for fields normal to the interfaces and not for fields applied parallel to them.

Assuming that the existence of superconductivity is the reason for the hysteresis in temperature, then the observed differences in the behavior of the FC-ZFC curves at different fields obtained for the HOPG-1 sample – relative to the those obtained for the WTGP – can be attributed to different superconducting phases. i.e. phases with different critical temperatures T_c 's, or difference pinning characteristics of the fluxons or vortices produced between or within the Josephson-coupled grains. At the stage of this research we are not able to provide any details on the pinning characteristics necessary to understand the $\Delta m(T, H)$ curves. Obviously, the pinning characteristics that these curves suggest are not simple and a description of the overall response has to take into account the Josephson coupling between the grains and the response of the superconducting single domains at fields above 40 mT, see Sec. 3.3. As a way to characterize the existence of different T_C 's or the overall pinning characteristics of the sample, we plot in Fig. 5 the temperature of the maxima observed in $\Delta m(T, H)$ in Fig. 3. Interestingly, their amplitude but not their position in temperature appears to depend on the applied field, see Fig. 5.

Experimental hints [35, 38, 40] as well as recent evidence [39] for the existence of embedded superconductivity at some interfaces in HOPG samples indicate that neither the critical temperature, nor the temperature below which a Josephson coupling between superconducting regions becomes effective, nor the distribution in space of the superconducting phase(s) in the

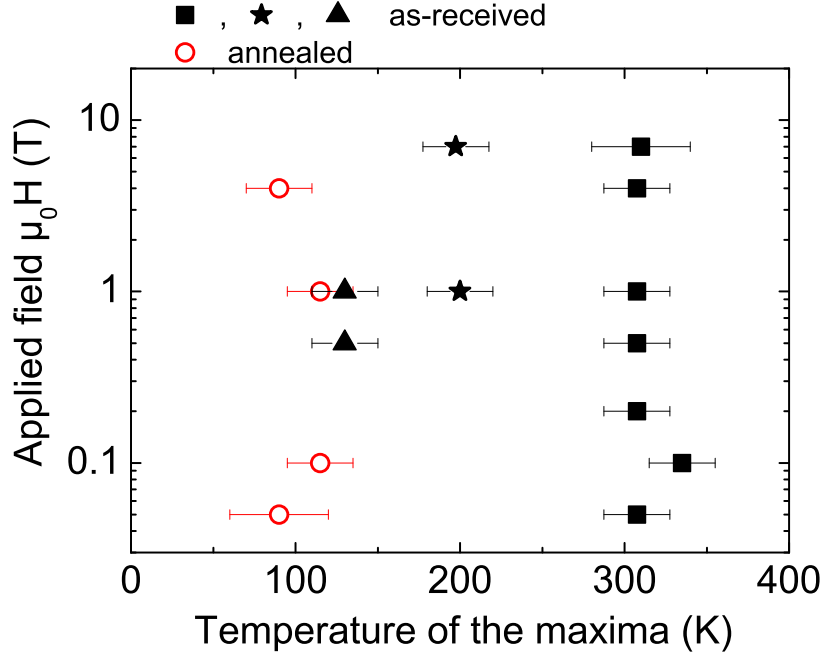


Figure 5: Temperature of the maxima obtained from the difference between FC and ZFC $\Delta m(T, H)$ curves vs. the applied field. The close symbols correspond to the sample in the as-received state and taken from Fig. 3 and the open symbol to the same sample HOPG-1 after annealing, see Fig. 12 in Sec. 3.4.

available HOPG samples is homogeneous. Therefore, one may speculate that the observed maxima could be also related to regions of the sample with different superconducting T_c 's.

Larger ZFC values (smaller in absolute value) than FC ones in the magnetic moment are rather exotic and usually not observed, neither in superconductors nor in ferromagnets and it is not known to be a SQUID artifact. To our knowledge this anomalous behavior in the FC-ZFC curves has been reported only for quasi-two-dimensional Ru-based weak ferromagnetic su-

perconductor [52] at one fixed magnetic field. The authors of that paper suggested an interplay and coexistence of superconductivity and weak ferromagnetic order as the origin for the anomaly but without providing more detail how this may work. Qualitatively speaking, we could speculate that this anomalous behavior is related to a magnetic p -wave order parameter [11] and that the superconducting properties can be enhanced to some extent under a magnetic field. In this case and upon the magnitude of the vortex of vortex/fluxon pinning, the FC curve could expel more field than the ZFC curve and a negative Δm is possible.

3.2. Magnetic field hysteresis

Field hysteresis loops for the two HOPG samples were measured at different temperatures. The total response of the samples for fields normal to the graphene layers is plotted in Fig. 6 at 300 K and for maximum applied fields of 40 mT and 50 mT for samples HOPG-1 and HOPG-2, respectively. The measurements of the field hysteresis start always at zero field after demagnetizing the sample at 390 K and cooling down at zero field to the measuring temperature. Within the scale of Fig. 6 one can recognize the field hysteresis for sample HOPG-1. The HOPG-2 sample shows no hysteresis within experimental resolution. Note that both samples show nearly identical diamagnetic magnetization values. The hysteresis due to the superconducting solenoid used by the SQUID apparatus produces a hysteresis artifact in the magnetic moment signal, which is proportional to the diamagnetic slope. This hysteresis is evident for fields above 100 mT in our apparatus, see Fig. 4 in the supplementary information in [32]. Taking also into account the larger mass of sample HOPG-2 (larger absolute diamagnetic slope), the results shown in

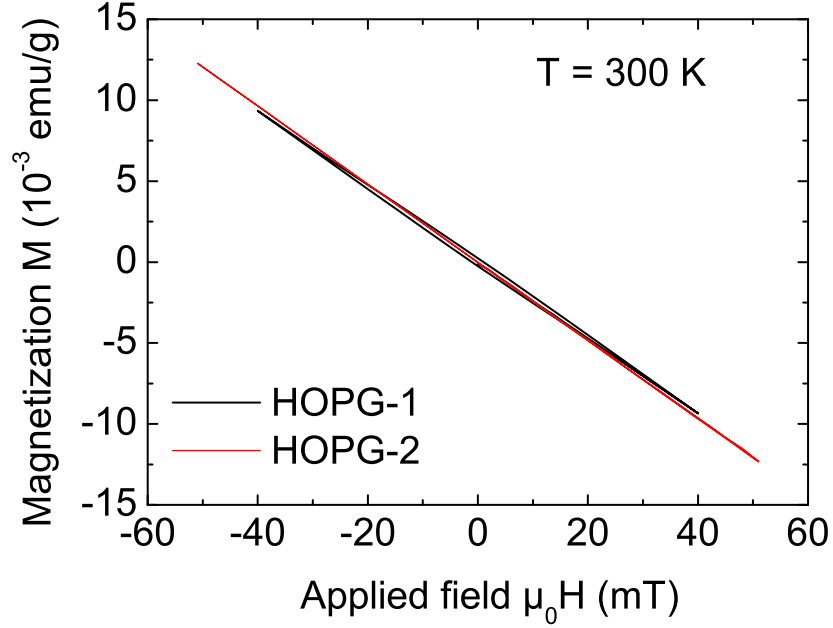


Figure 6: Magnetization field loops for samples HOPG-1 and HOPG-2 at 300 K. The field was applied normal to the graphene layers. The hysteresis is clearly seen in the scale of the figure for sample HOPG-1, whereas sample HOPG-2 shows no hysteresis within experimental error.

Fig. 6 indicate already that the field hysteresis found in sample HOPG-1 is not a SQUID artifact but it is intrinsic of the HOPG-1 sample.

After subtraction of the linear diamagnetic background ($m_D(5\text{K}) = 3.62 \times 10^{-5}$ emu/gOe and $m_D(300\text{K}) = 2.26 \times 10^{-5}$ emu/gOe for sample HOPG-1) the obtained hysteresis are plotted in Figs. 7 and 8 for $T = 5$ K and 300 K. For comparison the hysteresis of the WTGP [32] were included in the figures (right y -axis). The hysteresis for samples HOPG-1 and WTGP (S1), look similar whereas the HOPG-2 sample does not show any hysteresis at any temperature after subtracting a similar diamagnetic slope as for sample

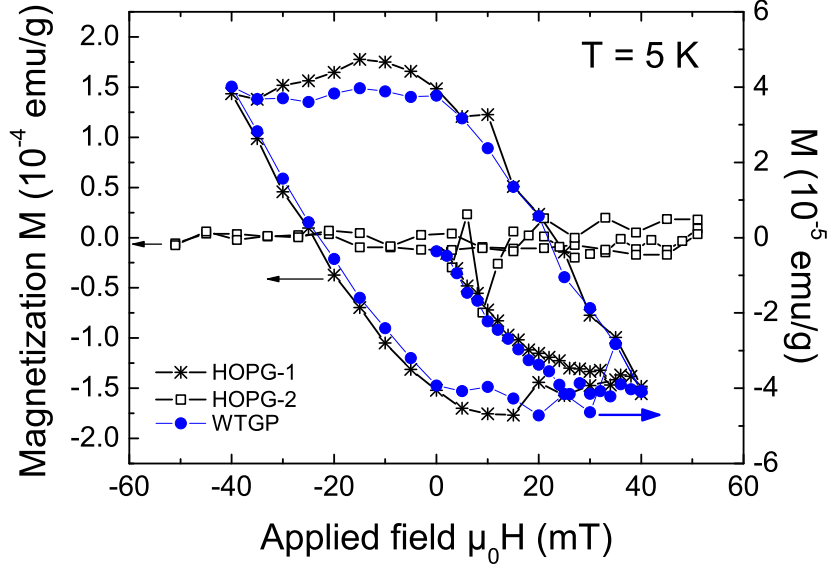


Figure 7: Magnetic field loops of the magnetization for fields applied normal to the graphene layers of the two HOPG samples (left y -axis) and of the WTGP (sample S1 from [32]) at 5 K. Linear diamagnetic backgrounds were subtracted from the measured signals.

HOPG-1. The obtained field hysteresis are superconductinglike and their shape depends on the maximum field applied as well as the temperature, compare the loops at Figs. 7 and 8. The hysteresis shape as well as its change with the maximum field in the loop are compatible with the existence of Josephson-coupled grains inside the HOPG-1 sample, in agreement with the current-voltage $I - V$ characteristic curves reported in [39] for TEM lamellae obtained from similar HOPG samples.

Note that the superconductinglike magnetization loops for the HOPG-1 sample, and for fields normal to the embedded interfaces, are about three to four times larger than the signals obtained for the WTGP sample. This

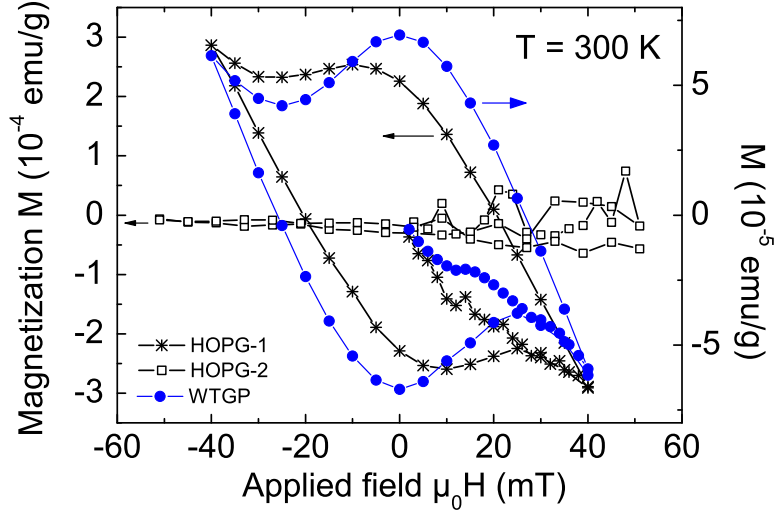


Figure 8: The same as in Fig. 7 but at $T = 300$ K after subtraction of the corresponding diamagnetic backgrounds, see Fig. 6.

should be not surprising since, firstly, we obtain the magnetization values dividing the superconductinglike magnetic moment by the total sample mass not by the superconducting mass and therefore no simple comparison can be really made. Second, due to the huge anisotropy in the magnetic field response and because the interfaces are distributed randomly with respect to the magnetic field in the case of the powder sample in contrast to the HOPG sample, we may expect smaller superconductinglike signals in the powder sample.

As pointed out above, at fields applied parallel to the graphene layers and to the interfaces there is no relevant hysteresis between the FC and ZFC curves in temperature nor as a function of applied field for both HOPG samples. This qualitative change in the magnetic response upon magnetic field

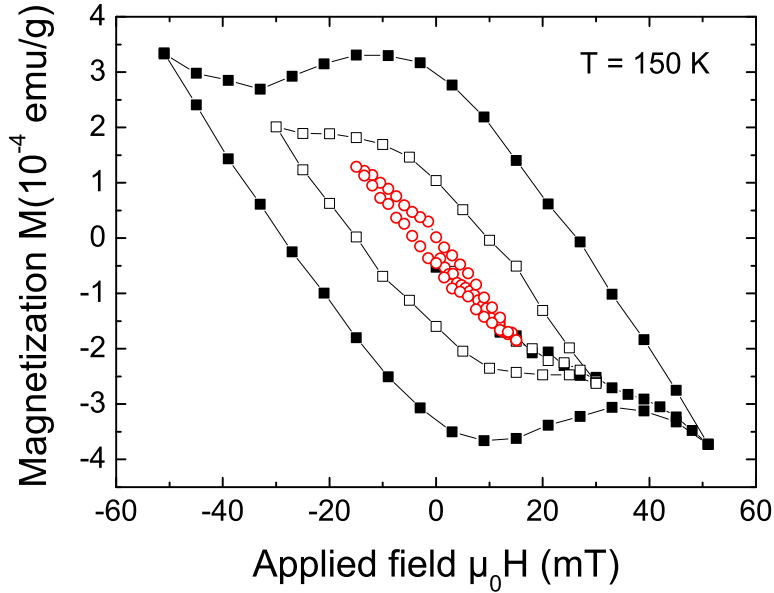


Figure 9: Magnetic moment as a function of field applied normal to the graphene planes and to the interfaces of sample HOPG-1 at 150 K. A constant diamagnetic slope was subtracted from the measured data. Each loop has been measured for a given maximum applied magnetic field.

direction has been already reported for bulk HOPG samples in [4]. The results presented here confirm at least part of those results and indicates clearly that the regions responsible for the measured signals run parallel to the graphene layers of the graphite sample. The clear two-dimensionality of the observed phenomenon rules out the possibility that the observed irreversibility in field or temperature is related to the existence of simple ferromagnetism in our sample, intrinsic or due to impurities, independently how small the ferromagnetic regions might be.

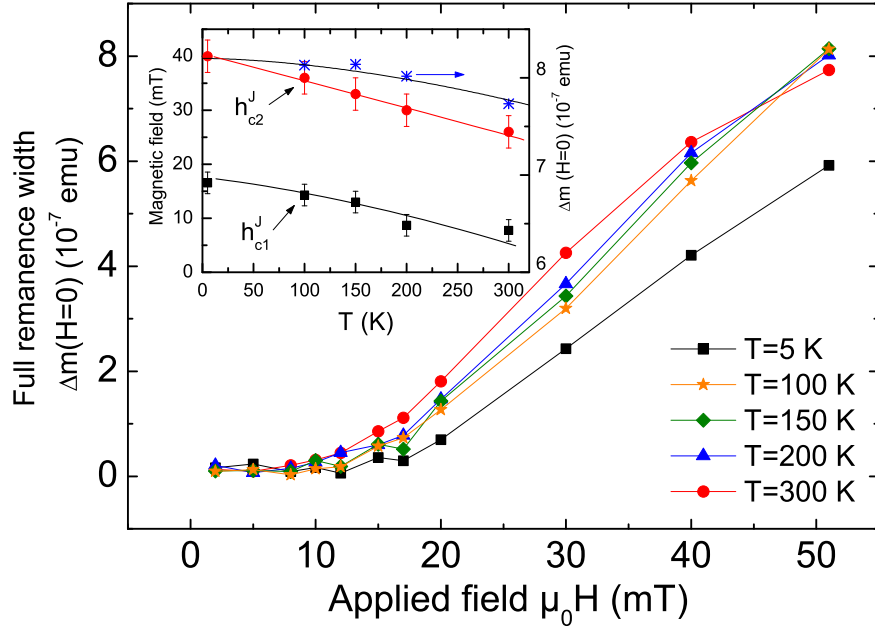


Figure 10: Full remanence width of the hysteresis loops $\Delta m(H = 0)$ measured after cycling the sample to a maximum field H_{\max} at different constant temperatures. The lower Josephson critical field h_{c1}^J shown in the insert (left y -axis) is defined at the crossing point between the zero line and a linear extrapolation of the increasing lines. Inset: Temperature dependence of the lower (close squares) and upper (close circles) critical Josephson fields (left y -axis). The lines through the points are an aid to the eye. The right y -axis corresponds to the full width of the hysteresis loop at zero field after cycling the field to $H_{\max} = 50$ mT. The blue curve follows $\Delta m(H = 0, T) = 0.82[\mu\text{emu}](1 - (T[\text{K}]/1700)^{1.7})$.

3.3. Josephson critical fields

As explained in [32, 53–55] and due to the granular superconductivity the magnetic field hysteresis of the magnetization changes its shape upon the maximum magnetic field applied at a given temperature. We expect to see a reversible, hysteresis free behavior below a certain Josephson-critical field $h_{c1}^J(T)$ to a Bean-like hysteresis at intermediate fields below the upper critical Josephson field $h_{c2}^J(T)$. An anomalous shrinking of the hysteresis plus a change in the slope of the virgin curve are observed at fields above $h_{c2}^J(T)$ [32, 53–55]. As an example, we show in Fig. 9 the hysteresis loops at 150 K obtained at different maximum applied fields for sample HOPG-1. The transition between a non-hysteretic, reversible region to an irreversible one occurs at $\mu_0 h_{c1}^J(150\text{K}) \simeq 12$ mT, in agreement with the next experiment described below.

The transition from reversible, zero remanence state to a finite remanence can be also recognized by determining directly the full remanence width at zero-field. In this case the remanent loop width at zero field is defined as $\Delta m(H = 0) = m_{H^+}(H = 0) - m_{H^-}(H = 0)$, i.e. coming from the positive H^+ or negative H^- field branches. Figure 10 shows $\Delta m(H = 0)$ as a function of H_{\max} at different constant temperatures. The whole behavior is similar to that measured for the WTGP [32] as well as in other high temperature superconductors [55, 56] and can be used to determine the Josephson critical field $h_{c1}^J(T)$, which temperature dependence is shown in the inset of this figure.

As in [32] we define $h_{c2}^J(T)$ at the beginning of the linear reversible region observed at high fields in the field loop measurements. The so obtained $h_{c2}^J(T)$

is shown in the inset of Fig. 10. Qualitatively speaking, the observed behavior for sample HOPG-1, for fields normal to the interfaces, is very similar to the one found for WTGP. The values of both Josephson critical fields as well as their ratio are very similar to those found for WTGP. However, the temperature dependence for $h_{c1,c2}^J(T)$ does not appear to follow a logarithmic one, as found for WTGP [32], but nearly a linear one. The temperature dependence of the full remanence width at $H = 0$ and after cycling the field to 50 mT is shown in the inset (right y -axis). Though qualitatively similar, $\Delta m(H = 0)(T)$ follows a slightly different temperature dependence as found for the WTGP, indicating also a critical temperature clearly above 300 K.

3.4. Annealing effects

After measuring the ZFC-FC and field hysteresis curves using the maximum allowed temperature for the SQUID ($T < 400$ K) we installed a SQUID oven, which enables measurements up to 800 K. The HOPG-1 sample was fixed with graphite glue (which gives a small diamagnetic contribution to the total signal) in a quartz glass capillary to avoid any contact with the oven inner wall. Before the measurements were started the oven was cleaned thoroughly and heated up to 800 K (without sample) for one hour to eliminate any possible magnetic contamination thereafter. The measurements were performed starting at 330 K with the same procedure as for the ZFC-FC curves described above. The measurements at all temperatures in the SQUID oven were performed in helium atmosphere.

In the first step and at 330 K we applied 50 mT field (always normal to the internal interfaces) to the previously demagnetized HOPG-1 sample and measured its magnetic moment up to 500 K (step 1) and back to the

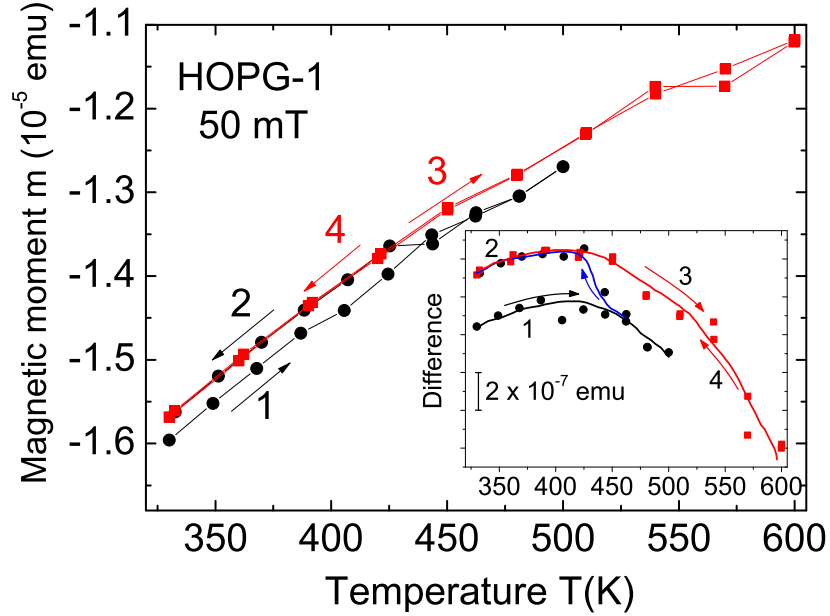


Figure 11: Temperature dependence of the magnetic moment of sample HOPG-1 at a field of 50 mT. The numbers and arrows indicate the order and direction of the temperature sweeps. The inset shows the same data as in the main panel but after subtraction of an arbitrary background line given by the equation $-1.12 \times 10^{-5} - 2 \times 10^{-8}(600 - T)$.

initial temperature (step 2). We should take into account that this kind of measurement, with a 25 K temperature step, implies an annealing to the sample. In particular, the sample was exposed to temperatures above 400 K for nearly one hour till its temperature decreased below 450 K. After the cycle $1 \rightarrow 2$, the procedure was repeated without changing the applied field but up to a maximum temperature of 600 K and back (steps 3 and 4). The results are shown in Fig. 11. In the inset of this figure we emphasize the observed irreversibility after the first step, subtracting an arbitrary background line. The opening of the curve between steps 1 and 2 can be clearly observed at

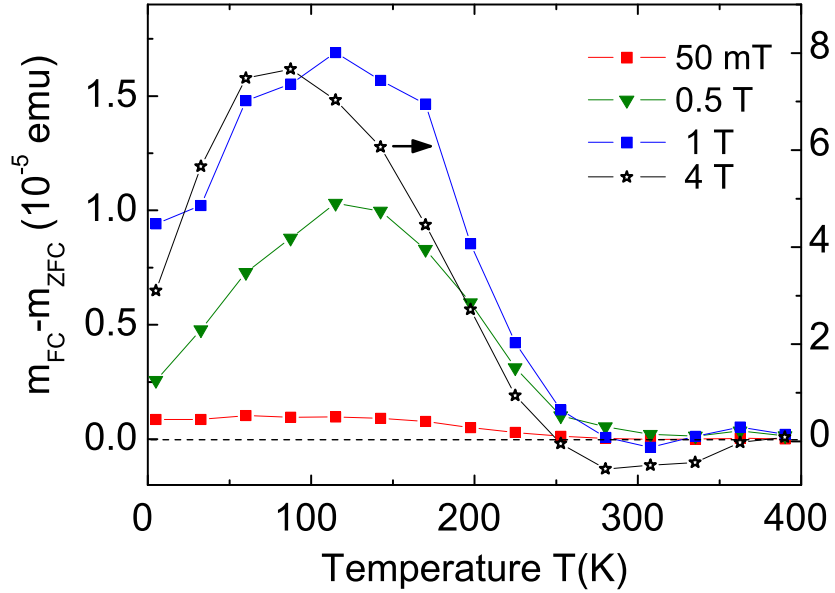


Figure 12: Difference between the FC and ZFC curves measured for sample HOPG-1 after annealing at different magnetic fields. The right y -axis corresponds to an applied field of 4 T.

~ 440 K indicating that part of the diamagnetic signal of the sample is lost after annealing. The second cycle 3 \rightarrow 4 with a maximum temperature of 600 K shows a reversible behavior following the same curve as that of step 2 below 425 K, see Fig. 11.

Figure 12 shows the difference between the FC and ZFC curves after step 4 and after removing the SQUID oven. The observed irreversible behavior at different applied fields has to be compared to the one obtained before annealing and shown in Fig. 3. It is clear that the annealing has produced a clear change in the irreversible behavior of the sample. For example, the irreversibility, which was observed at all fields from the highest temperature

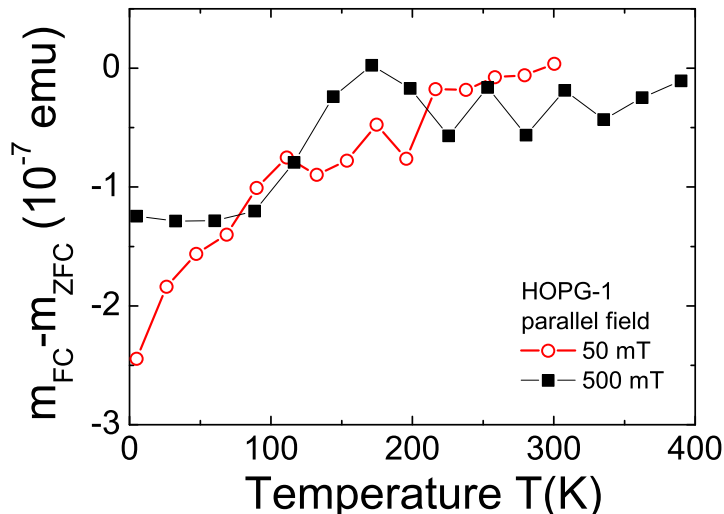


Figure 13: Difference between the FC and ZFC curves measured for sample HOPG-1 after annealing and for field applied parallel to the graphene layers of the sample.

turning point of 390 K, see Fig. 3, is shifted clearly below 300 K after annealing, see Fig. 12. The maxima observed at ~ 310 K and ~ 200 K (in the as-received HOPG-1 sample) vanish after annealing, leaving only an apparent single maximum at ~ 100 K, see Figs. 12 and 5. We note also that although the irreversibility temperature decreased below 300 K, the absolute difference at the maximum increased by a large factor.

If we interpret the change in the whole irreversibility in temperature after annealing as due to the vanishing or weakening of some superconducting phase and/or change in the pinning distribution or pinning strength, we may speculate on the following possibilities. Annealing at 500 K might change either the hydrogen concentration or simply the amount of defects at the interfaces in which superconductivity is embedded. An annealing temperature

of 500 K appears to be high enough to release strains and partially remove radiation damages in graphite [57]. On the other hand annealing can promote the formation of carbon clusters or the grow of other lattice phases [58] affecting either the pinning properties or the critical temperature. In case superconductivity would be solely related to the existence of interfaces between Bernal and rhombohedral phases [15], it appears highly unlikely that a temperature of 500 K or 600 K would affect them according to recently published studies [59].

To check whether the annealing did any change to the magnetic response of the sample for parallel fields, we have done ZFC and FC measurements at two applied fields. The magnetic field was applied parallel to the main area of the sample and parallel to its graphene layers and interfaces within $\pm 3^\circ$. Figure 13 shows the difference between the FC and ZFC curves. The difference remains mostly within experimental error of $\sim 10^{-7}$ emu, i.e. one to two orders of magnitude below the one obtained for the perpendicular field direction, see Fig. 12.

4. Conclusion

In this work we studied the magnetic response of a HOPG sample that shows similar irreversible behavior as the water treated graphite powders reported recently. As for those samples, the behavior observed in a HOPG sample in temperature and magnetic field appears to be compatible with the existence of high temperature granular superconductivity. In agreement with previous reports, this superconductinglike behavior is only observed for field normal to the internal interfaces (and to the graphene planes) of the

sample. Measurements in a similar HOPG sample with similar diamagnetic response but without interfaces do not show any irreversible behavior, neither in temperature nor as a function of magnetic field, ruling out obvious SQUID artifacts. Our results support the view that the superconducting phase(s) exist at or in embedded interfaces of the Bernal graphite matrix. The clear two dimensionality of the observed phenomenon rules out a ferromagnetic origin of the measured irreversibility. Because these interfaces are not found in all HOPG samples, our study provides an answer to the poor reproducibility of the superconductinglike signals in HOPG samples. Temperatures between 400 K and 600 K can change irreversibly the superconductinglike signals indicating that defects and/or hydrogen may play a role in the observed behavior.

Acknowledgements: This work is supported by the Deutsche Forschungsgemeinschaft under contract DFG ES 86/16-1.

References

- [1] Hannay NB, Geballe TH, Matthias BT, Andres K, Schmidt P, MacNair D. Superconductivity in graphitic compounds. *Phys Rev Lett* 1965;14:7.
- [2] Weller TE, Ellerby M, Siddharth SS, Smith RP, Skippe T. Superconductivity in the intercalated graphite compounds C_6Yb and C_6Ca . *Nature Phys* 2005;1:39–41.
- [3] Emery N, Hérold C, D’Astuto M, Garcia V, Bellin C, Marêché JF, et al. Superconductivity of bulk CaC_6 . *Phys Rev Lett* 2005;95:035413.
- [4] Kopelevich Y, Esquinazi P, Torres J, Moehlecke S. Ferromagnetic-

- and superconducting-like behavior of graphite. *J Low Temp Phys* 2000;119:691–702.
- [5] Esquinazi P, García N, Barzola-Quiquia J, Rödiger P, Schindler K, Yao JL, et al. Indications for intrinsic superconductivity in highly oriented pyrolytic graphite. *Phys Rev B* 2008;78:134516.
- [6] da Silva RR, Torres JHS, Kopelevich Y. Indication of superconductivity at 35 K in graphite-sulfur composites. *Phys Rev Lett* 2001;87:147001.
- [7] Kopelevich Y, da Silva RR, Torres JHS, Moehlecke S, Maple MB. High-temperature local superconductivity in graphite-sulfur composites. *Physica C* 2004;408:77–78.
- [8] Felner I, Kopelevich Y. Magnetization measurement of a possible high-temperature superconducting state in amorphous carbon doped with sulfur. *Phys Rev B* 2009;79:233409.
- [9] Kopelevich Y, Esquinazi P. Ferromagnetism and superconductivity in carbon-based systems. *J Low Temp Phys* 2007;146:629–639. and refs. therein.
- [10] Han SW, Lee JD, Noh JP, Jung DW. Superconductivity of a calcium-doped graphite CaC_{30} . *J Low Temp Phys* 2010;160:41–48.
- [11] González J, Guinea F, Vozmediano MAH. Electron-electron interactions in graphene sheets. *Phys Rev B* 2001;63:134421–1–8.
- [12] Nandkishore R, Levitov LS, Chubukov AV. Chiral superconductivity

- from repulsive interactions in doped graphene. *Nature Phys* 2012;8:158–163.
- [13] Black-Schaffer AM, Doniach S. Resonating valence bonds and mean-field d -wave superconductivity in graphite. *Phys Rev B* 2007;75:134512.
- [14] Kopnin NB, Heikkilä TT, Volovik GE. High-temperature surface superconductivity in topological flat-band systems. *Phys Rev B* 2011;83:220503.
- [15] Kopnin NB, Heikkilä TT. Surface superconductivity in rhombohedral graphite; 2012. ArXiv:1210.7075.
- [16] García N, Esquinazi P. Mean field superconductivity approach in two dimensions. *J Supercond Nov Magn* 2009;22:439–444.
- [17] Profeta G, Calandra M, Mauri F. Phonon-mediated superconductivity in graphene by lithium deposition. *Nature Phys* 2012;8:131–134.
- [18] Uchoa B, Neto AHC. Superconducting states of pure and doped graphene. *Phys Rev Lett* 2007;98:146801.
- [19] Kopnin NB, Sonin EB. BCS superconductivity of Dirac electrons in graphene layers. *Phys Rev Lett* 2008;100:246808.
- [20] Esquinazi P, Setzer A, Höhne R, Semmelhack C, Kopelevich Y, Spemann D, et al. Ferromagnetism in oriented graphite samples. *Phys Rev B* 2002;66:024429–1–10.

- [21] Esquinazi P, Spemann D, Höhne R, Setzer A, Han KH, Butz T. Induced magnetic ordering by proton irradiation in graphite. *Phys Rev Lett* 2003;91:227201–1–4.
- [22] Xia H, Li W, Song Y, Yang X, Liu X, Zhao M, et al. Tunable magnetism in carbon-ion-implanted highly oriented pyrolytic graphite. *Adv Mater* 2008;20:4679–4683.
- [23] Ohldag H, Tyliczszak T, Höhne R, Spemann D, Esquinazi P, Ungureanu M, et al. π -electron ferromagnetism in metal-free carbon probed by soft x-ray dichroism. *Phys Rev Lett* 2007;98:187204.
- [24] Zhang Y, Talapatra S, Kar S, Vajtai R, Nayak SK, Ajayan PM. First-principles study of defect-induced magnetism in carbon. *Phys Rev Lett* 2007;99:107201.
- [25] Yang X, Xia H, Qin X, Li W, Dai Y, Liu X, et al. Correlation between the vacancy defects and ferromagnetism in graphite. *Carbon* 2009;47:1399–1406.
- [26] Ohldag H, Esquinazi P, Arenholz E, Spemann D, Rothermel M, Setzer A, et al. The role of hydrogen in room-temperature ferromagnetism at graphite surfaces. *New Journal of Physics* 2010;12:123012.
- [27] Ugeda MM, Brihuega I, Guinea F, Gómez-Rodríguez JM. Missing atom as a source of carbon magnetism. *Phys Rev Lett* 2010;104:096804.
- [28] Yazyev OV. Emergence of magnetism in graphene materials and nanostructures. *Rep Prog Phys* 2010;73:056501.

- [29] Ramos MA, Barzola-Quiquia J, Esquinazi P, Muñoz Martin A, Climent-Font A, García-Hernández M. Magnetic properties of graphite irradiated with mev ions. *Phys Rev B* 2010;81(21):214404.
- [30] He Z, Yang X, Xia H, Zhou X, Zhao M, Song Y. Enhancing the ferromagnetism of graphite by successive $^{12}\text{C}^+$ ion implantation steps. *Carbon* 2011;49:1931–1938.
- [31] Miao X, Tongay S, Hebard A F. Extinction of ferromagnetism in highly ordered pyrolytic graphite by annealing. *Carbon* 2012;50:1614–1618.
- [32] Scheike T, Böhlmann W, Esquinazi P, Barzola-Quiquia J, Ballestar A, Setzer A. Can doping graphite trigger room temperature superconductivity? Evidence for granular high-temperature superconductivity in water-treated graphite powder. *Adv Mater* 2012;24:5826–5831.
- [33] Antonowicz K. Possible superconductivity at room temperature. *Nature* 1974;247:358–360.
- [34] Antonowicz K. The effect of microwaves on dc current in an al-carbon-al sandwich. *phys stat sol (a)* 1975;28:497–502.
- [35] Barzola-Quiquia J, Yao JL, Rödiger P, Schindler K, Esquinazi P. Sample size effects on the transport properties of mesoscopic graphite samples. *phys stat sol (a)* 2008;205:2924–2933.
- [36] García N, Esquinazi P, Barzola-Quiquia J, Dusari S. Evidence for semi-conducting behavior with a narrow band gap of Bernal graphite. *New Journal of Physics* 2012;14(5):053015.

- [37] Barzola-Quiquia J, Esquinazi P. Ferromagnetic- and superconducting-like behavior of the electrical resistance of an inhomogeneous graphite flake. *J Supercond Nov Magn* 2010;23:451–455.
- [38] Dusari S, Barzola-Quiquia J, Esquinazi P. Superconducting behavior of interfaces in graphite: Transport measurements of micro-constrictions. *J Supercond Nov Magn* 2011;24:401–405.
- [39] Ballestar A, Barzola-Quiquia J, Esquinazi P. Evidence of Josephson-coupled superconducting regions at the interfaces of highly oriented pyrolytic graphite; 2012. ArXiv:1206.2463.
- [40] Barzola-Quiquia J, Ballestar A, Dusari S, Esquinazi P. Experimental Study of the Intrinsic and Extrinsic Transport Properties of Graphite and Multigraphene Samples; chap. 8. Intech, Open Access Publisher, Jian Ru Gong (ed.); 2011,ISBN 978-953-307-292-0.
- [41] Reyren N, Thiel S, Caviglia AD, Kourkoutis LF, Hammerl G, Richter C, et al. Superconducting interfaces between insulating oxides. *Science* 2007;317:1196–1199.
- [42] Gozar A, Logvenov G, Kourkoutis LF, Bollinger AT, Giannuzzi LA, Muller LA, et al. High-temperature interface superconductivity between metallic and insulating copper oxides. *Nature* 2008;455:782–785.
- [43] Muntyanua F, Gilewski A, Nenkov K, Zaleski A, Chistol V. Superconducting crystallite interfaces with T_c up to 21 K in Bi and Bi-Sb bicrystals of inclination type. *Solid State Commun* 2008;147:183.

- [44] Esquinazi P, Barzola-Quiquia J, Spemann D, Rothermel M, Ohldag H, García N, et al. Magnetic order in graphite: Experimental evidence, intrinsic and extrinsic difficulties. *J Magn Magn Mat* 2010;322:1156–1161.
- [45] Ballestar A, Barzola-Quiquia J, Dusari S, Esquinazi P, da Silva RR, Kopelevich Y. Electric field induced superconductivity in multigraphene; 2012. ArXiv:1202.3327.
- [46] Lin Q, Li T, Liu Z, Song Y, He L, Hu Z, et al. High-resolution tem observations of isolated rhombohedral crystallites in graphite blocks. *Carbon* 2012;50:2347–2374.
- [47] Barzola-Quiquia J, Dusari S, Bridoux G, Bern F, Molle A, Esquinazi P. The influence of Ga^+ irradiation on the transport properties of mesoscopic conducting thin films. *Nanotechnology* 2010;21:145306.
- [48] Dusari S, Barzola-Quiquia J, Esquinazi P, García N. Ballistic transport at room temperature in micrometer-size graphite flakes. *Phys Rev B* 2011;83:125402.
- [49] Arndt A, Spoddig D, Esquinazi P, Barzola-Quiquia J, Dusari S, Butz T. Electric carrier concentration in graphite: Dependence of electrical resistivity and magnetoresistance on defect concentration. *Phys Rev B* 2009;80:195402.
- [50] McElfresh M, Li S, Sager R. Effects of magnetic field uniformity on the measurement of superconducting samples. Tech. Rep.; Quantum Design; 1994. Available at <http://www.qdusa.com/techsupport/index.html>.

- [51] Prozorov R, Yeshurun Y, Prozorov T, Gedanken A. Magnetic irreversibility and relaxation in assembly of ferromagnetic nanoparticles. *Phys Rev B* 1999;59:6956–6965.
- [52] Chiu TY, Lin YC, Tai MF, Lin BN, Guan PC, Chang BC, et al. High- T_c superconductivity in the new weak-ferromagnetic superconductor $\text{RuCa}_2\text{PrCu}_2\text{O}_{8+\delta}$. *Chinese Journal of Physics* 2005;43:616–622.
- [53] Senoussi S, Aguilon C, Hadjoudj S. The contribution of the intergrain currents to the low field hysteresis cycle of granular superconductors and the connection with the micro- and macrostructures. *Physica C* 1991;175:215–225.
- [54] Borik M, Chernikov M, Veselago V, Stepankin V. Anomalies of the magnetic properties of granular oxide superconductor $\text{BaPb}_{1-x}\text{Bi}_x\text{O}_3$. *J Low Temp Phys* 1991;85:283–294.
- [55] Andrzejewski B, Guilmeau E, Simon C. Modelling of the magnetic behaviour of random granular superconductors by the single junction model. *Supercond Sci Technol* 2001;14:904–909.
- [56] McElfresh MW, Yeshurun Y, Malozemoff AP, Holtzberg F. Remanent magnetization, lower critical fields and surface barriers in an $\text{YBa}_2\text{Cu}_3\text{O}_7$ crystal. *Physica A* 1990;168:308–318.
- [57] Primak W. Annealing of radiation damage in graphite. *J Appl Phys* 1978;49:4761–4764.
- [58] Bollmann W. Electron-microscopy observations on radiation damage in graphite. *J Appl Phys* 1961;32:869–876.

- [59] Lui CH, Li Z, Chen Z, Klimov PV, Brus LE, Heinz TF. Imaging stacking order in few-layer graphene. *Nano Lett* 2011;11:164–169.